

Testing chiral unitary models for the $\Lambda(1405)$ in $K^+\pi\Sigma$ photoproduction

P. C. Bruns,^{1,*} A. Cieplý,^{1,†} and M. Mai^{2,3,‡}

¹*Nuclear Physics Institute of the Czech Academy of Sciences, 250 68 Řež, Czechia*

²*Helmholtz-Institut für Strahlen- und Kernphysik (Theorie) and Bethe Center for Theoretical Physics, Universität Bonn, D-53115 Bonn, Germany*

³*The George Washington University, Washington, DC 20052, USA*



(Received 23 June 2022; accepted 27 September 2022; published 17 October 2022)

We adopt a novel formalism for the low-energy analysis of the $\gamma p \rightarrow K^+\pi\Sigma$ photoproduction reaction, outlined recently in [P. C. Bruns, [arXiv:2012.11298](https://arxiv.org/abs/2012.11298)], to calculate the $\pi\Sigma$ invariant mass distributions in the $\Lambda(1405)$ resonance region. The approach adheres to constraints arising from unitarity, gauge invariance, and chiral perturbation theory, and is used without adjusting any model parameters. It is found that the meson-baryon rescattering in the final state has a major impact on the magnitude and structure of the generated spectra that are compared with the experimental data from the CLAS Collaboration. We demonstrate a large sensitivity of the theoretical predictions to the choice of the coupled-channel $\pi\Sigma - \bar{K}N$ model amplitudes which should enable one to constrain the parameter space of these models.

DOI: [10.1103/PhysRevD.106.074017](https://doi.org/10.1103/PhysRevD.106.074017)

I. INTRODUCTION

Unraveling the general patterns and the nature of individual (excited) states in the hadron spectrum is essential to test our understanding of the strong interaction. Within that, only few other states have such a long-lasting history as the enigmatic $\Lambda(1405)$ resonance, becoming a benchmark for our understanding of the SU(3) hadron dynamics. Starting with its theoretical prediction [1] and later experimental verification [2], until the most recent debates on the existence of the second broad pole, it emerged as a fruitful research area sparking many theoretical and experimental developments. For a deeper recap of the character and history of $\Lambda(1405)$, established to be an $I(J^P) = 0(1/2^-)$ resonance in the strangeness $S = -1$ sector, we refer the reader to the recent dedicated reviews [3,4]. More general reviews of our present understanding of excited hadrons can be found in Refs. [5,6].

Broader impact of the research related to the antikaon-nucleon systems includes the following: (1) Application to the $\Lambda_b \rightarrow J/\psi\Lambda(1405)$ decay [7] and similar processes with the final-state interaction dominated by the nonperturbative meson-baryon dynamics [8]; (2) investigation of and search for \bar{K} nuclei ($\bar{K}NN$, $\bar{K}KN$, $\bar{K}NNN$, etc.), being part of large experimental programs at DAΦNE [9,10], Saclay [11–13] or at J-PARC [14,15] to name just a few; (3) the exploration of the in-medium properties of antikaons and strange nuclear matter [16–18]. One natural application is also

represented by studies of the equation of state of neutron stars in relation to the strangeness; see the comprehensive review [19] on many aspects related to strangeness in nuclear physics.

The state-of-the-art theoretical approaches to the universal parameters of the subthreshold $\Lambda(1405)$ resonance include various forms of coupled-channel models implementing S -matrix unitarity, while also adding constraints from chiral symmetry of QCD to various degrees. Parameters of such models are typically fixed by fitting K^-p reactions and threshold data, and the chirally motivated coupled-channel dynamics generates two poles in the complex energy plane [20–23]. The theoretical predictions [24–28] tend to agree on the position of the narrow pole located around 1425 MeV, coupling strongly to the $\bar{K}N$ channel and mostly interpreted as a meson-baryon molecular state. The position of the second pole is not determined so well, but seems to lie at lower energies and deeper in the complex energy-plane. This so-called *double-pole* structure of $\Lambda(1405)$ is what makes this state particularly curious, while we know now that such a structure is common to many other states in the hadron spectrum [6,29].

One particular complication in accessing the parameters of both $\Lambda(1405)$ states directly lies in the fact that there is no Σ target to perform $\pi\Sigma$ scattering experiments. This hurdle can be overcome by analyzing processes with $\pi\Sigma$ appearing in the final state. This is the case, e.g., for the *two-meson photoproduction* reaction $\gamma p \rightarrow K^+\pi\Sigma$ in which the K^+ meson takes away momentum, enabling a scan in the invariant mass of the $\pi\Sigma$ system down to its production threshold. Such determined line shape of the $\pi\Sigma$ system covers the relevant energy and, in principle, allows one to

*bruns@ujf.cas.cz

†cieply@ujf.cas.cz

‡mai@hiskp.uni-bonn.de

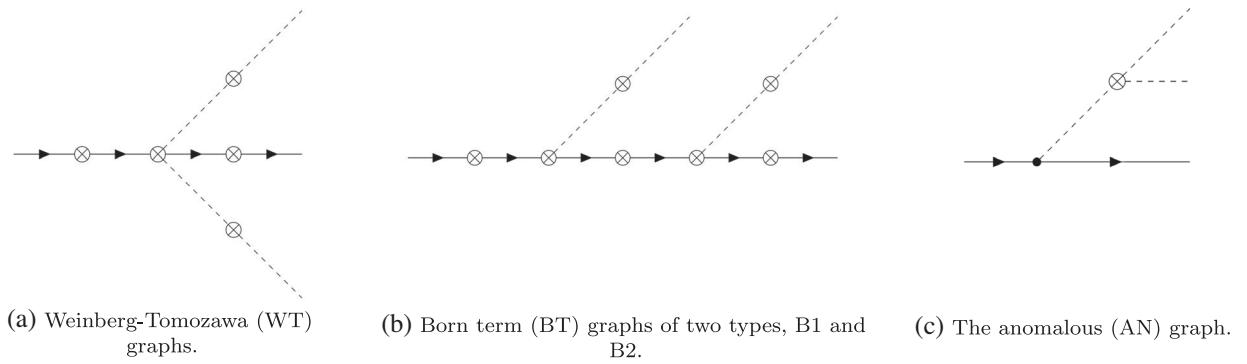


FIG. 1. Three classes of tree graphs for the two-meson photoproduction amplitude. Directed lines: baryons, dashed lines: pseudoscalar mesons, crossed circles: possible photon insertions. Working at order $\mathcal{O}(e)$, the first figure (a) represents five graphs, each with the photon attached to a different crossed vertex. The same notation system applies to figures (b) and (c) giving altogether rise to $5 + (2 \times 7) + 1 = 20$ tree graphs.

extract the parameters of the $S = -1$ meson-baryon system more directly. The corresponding experiment was performed by the CLAS Collaboration several years ago, taking very precise, high-resolution data [30–32]. These data have already made a significant impact on the field; see Refs. [26,33–39], where various photoproduction models have been tested and the generated $\pi\Sigma$ mass distributions compared with the data. Our work aims to contribute to these efforts by implementing a recently proposed formalism [40] for the $\gamma p \rightarrow K^+ \pi \Sigma$ transition and discussing the sensitivity of the calculated cross sections to ambiguities inherent in extending the $\pi\Sigma - \bar{K}N$ coupled-channel models to energies below the $\bar{K}N$ threshold. In the future, this should allow us to reduce the model dependence and shrink the parameter space at the same time.

At this point, it might be appropriate to mention other contemporary and ongoing experimental studies aiming at shedding more light on this enigmatic part of the hadron spectrum. First of all, the $\pi\Sigma$ mass spectra were also measured in other reactions, some of them compatible with the CLAS data [41,42] and some others not [43]. Completely new experimental data on the isoscalar $\pi^0 \Sigma^0$ photoproduction should also be reported soon by the GlueX Collaboration [44]. Other efforts aim at determining the isovector part of the $\bar{K}N$ interaction via precise measurements of the kaonic hydrogen and kaonic deuterium characteristics [45–47] or by studying the related $K_L^0 p \rightarrow K^+ \Xi^0$ reaction [48]. Finally, exciting new prospects in exploring strangeness in the hadron spectrum may open with the PANDA experiment [49,50].

The article is organized as follows: In Sec. II we introduce the formalism adopted to study the $K^+ \pi \Sigma$ photoproduction on proton targets. In Sec. III we discuss the predictions¹ made using this formalism, and compare

the resulting $\pi\Sigma$ mass distributions with the CLAS data. Finally, in Sec. IV we conclude by summarizing our findings and provide an outlook for future directions.

II. FORMALISM

We consider the two-meson photoproduction reaction $\gamma(k)p(p_N) \rightarrow K(q_K)\pi(q_\pi)\Sigma(p_\Sigma)$, where the symbol in brackets denotes the four-momentum of the indicated particle. For a process with five external particles, we can form five independent Mandelstam variables, which we choose here as

$$\begin{aligned} s &= (p_N + k)^2 = (q_K + q_\pi + p_\Sigma)^2, \\ M_{\pi\Sigma}^2 &= (q_\pi + p_\Sigma)^2, \quad t_\Sigma = (p_\Sigma - p_N)^2, \\ u_\Sigma &= (p_\Sigma - k)^2, \quad t_K = (q_K - k)^2. \end{aligned} \quad (2.1)$$

The two-meson photoproduction amplitude can be decomposed as

$$\begin{aligned} \mathcal{M}^\mu &= \gamma^\mu \mathcal{M}_1 + p_N^\mu \mathcal{M}_2 + p_\Sigma^\mu \mathcal{M}_3 + q_K^\mu \mathcal{M}_4 \\ &+ \not{k} (\gamma^\mu \mathcal{M}_5 + p_N^\mu \mathcal{M}_6 + p_\Sigma^\mu \mathcal{M}_7 + q_K^\mu \mathcal{M}_8) \\ &+ \not{q}_K (\gamma^\mu \mathcal{M}_9 + p_N^\mu \mathcal{M}_{10} + p_\Sigma^\mu \mathcal{M}_{11} + q_K^\mu \mathcal{M}_{12}) \\ &+ \not{q}_K \not{k} (\gamma^\mu \mathcal{M}_{13} + p_N^\mu \mathcal{M}_{14} + p_\Sigma^\mu \mathcal{M}_{15} + q_K^\mu \mathcal{M}_{16}), \end{aligned} \quad (2.2)$$

where we have suppressed structures $\sim k^\mu$ that do not contribute to the photoproduction cross section. The structures \mathcal{M} can be obtained diagrammatically as it is shown explicitly in Appendix C of Ref. [40]. At the leading order (LO), there are 20 tree level diagrams contributing to these structures as depicted in Fig. 1. These can be arranged in three classes: (WT) graphs with one Weinberg-Tomozawa contact term with a photon attached to one of five possible places; (B1/B2) Born graphs with the pion/kaon emitted before the kaon/pion, respectively, including seven possible photon coupling possibilities; (AN) graphs with a

¹One might be inclined to speak of *retrodictions*, but we prefer the more common word *predictions* used here when specific model simulations are confronted with already existing data.

three-meson-photon vertex from the anomalous Wess-Zumino-Witten Lagrangian [51,52]. Thus, $5 + (2 \times 7) + 1 = 20$ tree diagrams comprise our photoproduction kernel. We also remark that the latter class of graphs yields contributions of subleading chiral order in the low-energy power counting, but we include it here as a test of higher-order contributions, without introducing new adjustable parameters.

Our notation for kinematics is such that Lorentz-non-invariant quantities (like angles and three-momenta) are marked with a $(*)$ if they are evaluated in the $\pi\Sigma$ c.m. frame (where $\vec{p}_\Sigma^* + \vec{q}_\pi^* = \vec{0}$), and otherwise refer to the overall c.m. frame where $\vec{p}_N + \vec{k} = \vec{0}$. For example, we have

$$|\vec{q}_K| = \frac{\sqrt{\lambda(s, M_{\pi\Sigma}^2, M_K^2)}}{2\sqrt{s}}, \quad (2.3)$$

$$|\vec{p}_\Sigma^*| = \frac{\sqrt{\lambda(M_{\pi\Sigma}^2, m_\Sigma^2, M_\pi^2)}}{2M_{\pi\Sigma}}, \quad (2.4)$$

employing $\lambda(x, y, z) := x^2 + y^2 + z^2 - 2xy - 2xz - 2yz$.

In the coupled-channel formalism of *unitarized ChPT*, one constructs meson-baryon partial-wave scattering amplitudes $f_{\ell^\pm}^{c',c}(M_{\pi\Sigma})$, which aim to describe the scattering from channel c to channel c' (here, $c, c' = \pi\Sigma, \bar{K}N, \eta\Lambda, \dots$) for total angular momentum $\ell \pm \frac{1}{2}$ and orbital angular momentum $\ell = 0, 1, 2, \dots$. These amplitudes are designed in such a way to be consistent with ChPT up to a fixed order of the low-energy expansion [in practice, usually on tree level, i.e., $\mathcal{O}(p)$ or $\mathcal{O}(p^2)$]. At the same time, they fulfill the requirement of coupled-channel unitarity,

$$\text{Im}(f_{\ell^\pm}) = (f_{\ell^\pm})^\dagger (|\vec{p}^*|) (f_{\ell^\pm}), \quad (2.5)$$

above the lowest reaction threshold. Here, f_{ℓ^\pm} denotes a complex-valued matrix in the space of the considered meson-baryon channels c, c' , with entries $f_{\ell^\pm}^{c',c}(M_{\pi\Sigma})$, while $(|\vec{p}^*|)$ is a diagonal matrix in this space, the entries of which are given by the moduli of the three-momenta (for each channel c) in the meson-baryon c.m. frame [see Eq. (2.4)] above the threshold of channel c and zero below it.

It is our aim to implement the scattering amplitudes f_{0+} in the photoproduction formalism in such a way, that it describes the final-state s -wave interaction of the $S = -1$ meson-baryon pair (MB) produced in the $\gamma p \rightarrow K^+ MB$ reaction as illustrated in Fig. 2. Clearly, we have to find the combinations of (partial-wave projections of) the structure functions $\mathcal{M}_{i=1,\dots,16}$ which project on the $\ell = 0$ state of this meson-baryon pair. In fact, one can construct projected photoproduction amplitudes $\mathcal{A}_{0+}^{i=1,\dots,4}(s, M_{\pi\Sigma}^2, t_K)$ from the \mathcal{M}_i , which have simple unitarity relations with the pertinent s -wave scattering amplitudes,

$$\text{Im}(\mathcal{A}_{0+}^i) = (f_{0+})^\dagger (|\vec{p}^*|) (\mathcal{A}_{0+}^i), \quad i = 1, \dots, 4. \quad (2.6)$$

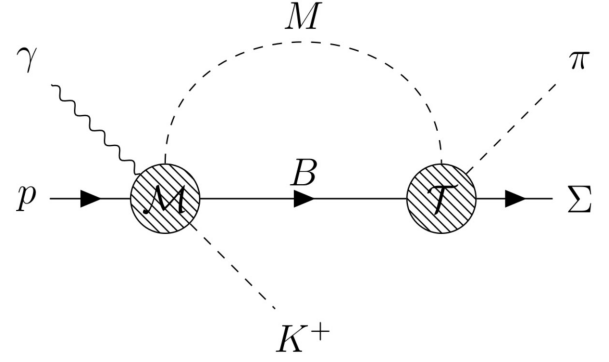


FIG. 2. Representation of the final-state interaction of the $S = -1$ meson-baryon pair MB . \mathcal{M} is the amplitude for $\gamma p \rightarrow K^+ MB$ without final-state interaction, and \mathcal{T} is the $S = -1$ meson-baryon scattering amplitude, which can be decomposed into partial waves f_{ℓ^\pm} [54].

Note that there are *four* amplitudes for the production of a state with $\pi\Sigma$ being in an s -wave, corresponding to the four invariant amplitudes for the photoproduction process $\gamma p \rightarrow K^+ \Lambda^*$; see Ref. [40] for more details. The projections \mathcal{A}_{0+}^i can be found, e.g., by applying the Cutkosky rules [53] to the MB loop in Fig. 2, and studying the consequences of unitarity for the various invariant structures in \mathcal{M}^μ . More specifically, we consider the coupled-channel unitarity constraint $\text{Im}\mathcal{M}^\mu = \mathcal{T}^\dagger G_{\text{Cut}} \mathcal{M}^\mu$, where G_{Cut} is obtained from the MB loop function by replacing the propagators according to

$$(p^2 - m^2 + i\epsilon)^{-1} \rightarrow -2\pi i \Theta(p^0) \delta(p^2 - m^2), \quad (2.7)$$

where $\Theta(\cdot)$ denotes the Heaviside step function and $\delta(\cdot)$ the Dirac delta function. Note that, due to this replacement, only on-shell amplitudes \mathcal{M}^μ and \mathcal{T} enter the expression for $\text{Im}\mathcal{M}^\mu$. \mathcal{M}^μ comprises 16 invariant amplitudes as given in Eq. (2.2), while there are two structures in \mathcal{T} and G_{Cut} . The coefficients of the operator structures can be matched on both sides of the coupled-channel unitarity constraint. This yields a system of equations which can, after some lengthy algebra, be brought into a partial-wave projected form like in Eq. (2.6), making use of the well-known partial-wave expansion of the MB on-shell scattering amplitude \mathcal{T} [54]. Equivalently, one can employ the methods used in Ref. [55–57] to extract the multipole amplitudes for single-meson photoproduction (we have verified explicitly that both methods also agree for the case of single-meson photoproduction).

Explicit expressions for the \mathcal{A}_{0+}^i are provided in the Appendix. This analysis is somewhat simplified, employing an approximation which is motivated by the observations made in Sec. 4 of Ref. [40]. In that, confining ourselves to a low-energy analysis in the $\Lambda(1405)$ energy region, it is reasonable to neglect higher partial waves $\sim \mathcal{Y}_{\ell>0,m}(\theta_\Sigma^*, \phi_\Sigma^*)$

in the decomposition of the \mathcal{M}_i into spherical harmonics, and express the projections solely through

$$\bar{\mathcal{M}}_i(s, M_{\pi\Sigma}^2, t_K) := \int \frac{d\Omega_{\Sigma}^*}{4\pi} \mathcal{M}_i(s, M_{\pi\Sigma}^2, t_K, t_{\Sigma}, u_{\Sigma}). \quad (2.8)$$

The s -wave resonance pole terms in the photoproduction amplitude are not affected by this approximation. We also note that this approximation can be used for any c.m. energy \sqrt{s} , as long as $M_{\pi\Sigma}$ stays sufficiently close to the MB threshold region. Therefore, kinematics involving high-energy kaons can, in principle, be treated within the framework of this section. Of course, the ChPT tree graphs

might not be sufficient for this purpose, and the elementary photoproduction amplitude would have to be amended.

Neglecting contributions due to the $\pi\Sigma$ states with $\ell > 0$, the double-differential cross section for the $\gamma p \rightarrow K^+ \pi\Sigma$ reaction can be expressed through the \mathcal{A}_{0+}^i amplitudes as follows:

$$\frac{d^2\sigma}{d\Omega_K dM_{\pi\Sigma}} = \frac{|\vec{q}_K| |\vec{p}_{\Sigma}^*|}{(4\pi)^4 s |\vec{k}|} |\mathcal{A}|^2, \quad (2.9)$$

where we introduced

$$\begin{aligned} 4|\mathcal{A}|^2 &= (1 - z_K) |\mathcal{A}_{0+}^1 + \mathcal{A}_{0+}^2|^2 + (1 + z_K) |\mathcal{A}_{0+}^1 - \mathcal{A}_{0+}^2|^2 \\ &+ (1 - z_K) \left| \mathcal{A}_{0+}^1 + \mathcal{A}_{0+}^2 + \frac{2|\vec{q}_K|(1 + z_K)}{M_K^2 - t_K} ((\sqrt{s} + m_N)\mathcal{A}_{0+}^3 + (\sqrt{s} - m_N)\mathcal{A}_{0+}^4) \right|^2 \\ &+ (1 + z_K) \left| \mathcal{A}_{0+}^1 - \mathcal{A}_{0+}^2 - \frac{2|\vec{q}_K|(1 - z_K)}{M_K^2 - t_K} ((\sqrt{s} + m_N)\mathcal{A}_{0+}^3 - (\sqrt{s} - m_N)\mathcal{A}_{0+}^4) \right|^2, \end{aligned}$$

with $z_K \equiv \cos \theta_K$, θ_K being the angle between \vec{q}_K and \vec{k} in the overall c.m. frame.

Returning to the partial-wave unitarity statement in Eq. (2.6), the proposed coupled-channel formalism is now easily explained. We have to construct an elementary photoproduction amplitude, e.g., from the tree graphs discussed above, computing the according projected amplitudes $\mathcal{A}_{0+}^{i(\text{tree})}$, as detailed. Since we treat the outgoing K^+ effectively as a spectator particle in our unitarization procedure, as was also done in previous studies [26,33–35,58,59], the final-state interaction in our model is restricted to the $S = -1$ meson-baryon subspace, which is the relevant sector for the formation of the $\Lambda(1405)$. Therefore, unitarized amplitudes for $\gamma p \rightarrow K^+ MB$ will be taken as the coupled-channel vector

$$(\mathcal{A}_{0+}^i) = (\mathcal{A}_{0+}^{i(\text{tree})}) + (f_{0+}) (8\pi M_{\pi\Sigma} G(M_{\pi\Sigma})) (\mathcal{A}_{0+}^{i(\text{tree})}). \quad (2.10)$$

Here, $G(M_{\pi\Sigma})$ is a diagonal channel-space matrix, with entries given by suitably regularized loop integrals

$$\begin{aligned} iG^{c=MB}(M_{\pi\Sigma}) &= \int_{\text{reg}} \frac{d^4 l}{(2\pi)^4} \frac{1}{((p_{\Sigma} + q_{\pi} - l)^2 - m_B^2 + i\epsilon)(l^2 - M_M^2 + i\epsilon)}. \end{aligned} \quad (2.11)$$

The $MB = \pi\Sigma$ entries of the vector \mathcal{A}_{0+}^i can then be inserted in formula (2.9) to obtain the required s -wave cross sections. Using the fact that

$$8\pi M_{\pi\Sigma} \text{Im} G^{MB}(M_{\pi\Sigma}) = |\vec{p}_B^*| \Theta(M_{\pi\Sigma} - m_B - M_M), \quad (2.12)$$

together with Eq. (2.5), it is straightforward to show that the ansatz (2.10) solves the unitarity requirement (2.6).

In the actual calculations presented in the next section we will use f_{0+} amplitudes generated by two different approaches to MB coupled-channel interactions. Both of them derive the interaction kernel from the MB chiral Lagrangian taken up to the NLO order, but differ (among other details) in the methods adopted to regularize the loop function G . In order to stay consistent with the construction of the amplitudes, we will use in each case the appropriate regulation procedure that is employed in the respective model. Thus, in the case of the Bonn models presented in Refs. [26,60], we take the dimensionally regularized integral $G = -I_{MB}$ (see Appendix B of [40]), while in the case of the Prague model [28], we take the loop integral of Eq. (8) in [61], divided by $8\pi M_{\pi\Sigma} g_{jb}^2$, to conform with Eq. (2.12). Requiring that both versions of the loop function G agree at the threshold energy $M_{MB} = m_B + M_M$ yields a matching relation between the regulator scale α used in Refs. [28,61] and the mass scale μ adopted in Refs. [26,60]:

$$\pi\alpha \stackrel{!}{=} m_B + M_M - m_B \log\left(\frac{m_B^2}{\mu^2}\right) - M_M \log\left(\frac{M_M^2}{\mu^2}\right). \quad (2.13)$$

For a *natural* scale of $\mu \approx 1$ GeV used in dimensional regularization this somewhat *ad-hoc* matching procedure provides $\alpha_{\pi\Sigma} \approx 460$ MeV and $\alpha_{\bar{K}N} \approx 715$ MeV, both values obtained via Eq. (2.13) at the respective channel thresholds.

After ensuring two-body unitarity in the final state we turn to another aspect, the gauge invariance of the photoproduction amplitude. Could there be a conflict between Eqs. (2.9) and (2.10) and gauge invariance? The answer is not trivial. Even a gauge-invariant tree-level amplitude $\mathcal{M}_{(\text{tree})}^\mu$ does not necessarily generate a gauge-invariant unitarized amplitude when it is just plugged into a loop integral to couple it to the final-state interaction, since it will usually depend on the loop momentum that is integrated over. We refer here to the discussions in [62–65]; see also Refs. [66,67]. In our present framework, the issue is resolved as follows. Given the functions $\mathcal{A}_{0+}^i(s, M_{\pi\Sigma}^2, t_K)$, we can find a set of invariant amplitudes \mathcal{M}_i^C (provided in the Appendix) which form a gauge-invariant amplitude by construction, and yield the same projections \mathcal{A}_{0+}^i . The s -wave cross section calculated directly from this gauge-invariant amplitude exactly equals the one in Eq. (2.9). The difference between the invariant amplitudes, thus, resides in the higher meson-baryon partial waves. This strategy works for every gauge-invariant set of $\mathcal{A}_{0+}^{i(\text{tree})}$ in (2.10), which allows for some flexibility in the construction of models for these functions. For example, we could add higher-order contact terms to the ChPT tree graphs. All these models will yield cross sections that are in accord with s -wave coupled-channel unitarity, gauge invariance, and the chiral low-energy theorems [40] (as long as the model used for the f_{0+} does not spoil the proper low-energy behavior) at the same time.

III. COMPARISON WITH DATA

We use the formalism described in the previous section to calculate the $\pi\Sigma$ mass distributions observed in the CLAS experiment [30] for the photoproduction reactions on a proton target.

First, we look at the relevance of various contributions to the s -wave amplitude of the photoproduction process. In Fig. 3 we present the results obtained for the mass spectra at $W = \sqrt{s} = 2.0$ GeV when only the tree-level graphs contribute to the amplitude, and demonstrate the additional impact of including the MB rescattering in the final state. For the latter, we have adopted only the recent version of the $\bar{K}N$ Prague model [28] to generate the rescattering amplitudes f_{0+} required in Eq. (2.10), but will present results including more models below. We observe that when only the WT tree graph is considered (dotted red lines in the figure), without the rescattering second term of Eq. (2.10), the $\pi\Sigma$ cross sections are either exactly zero (for $\pi^+\Sigma^-$),² quite negligible (for $\pi^0\Sigma^0$), or remain very small (for $\pi^-\Sigma^+$). The addition of Born and anomalous terms

²This result is caused by a structure of the WT graph in this case.

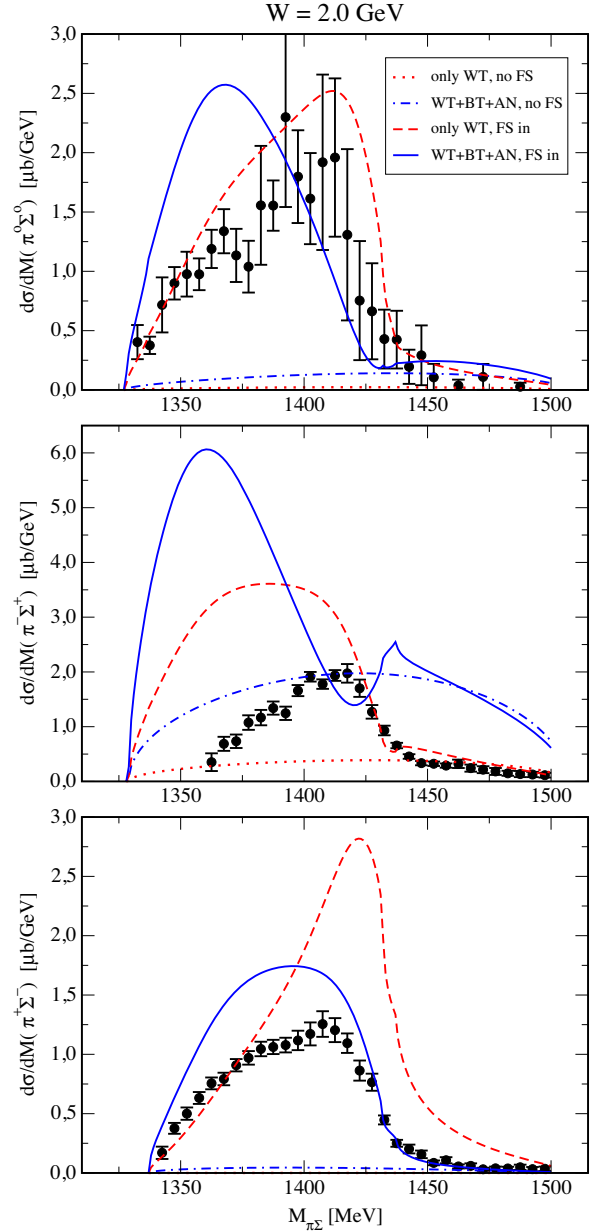


FIG. 3. The calculated $\pi\Sigma$ mass distributions are compared with experimental data taken from [30]. The lines demonstrate the contributions from WT and other (BT + AN) graphs, and the impact of the MB rescattering in the final state.

leads to larger cross sections (shown by dot-dashed blue lines in the figure). However, only in the $\pi^-\Sigma^+$ channel does the predicted mass distribution compare in magnitude with the one observed in the CLAS experiment [30]. It should be noted that all three $\pi\Sigma$ mass distributions generated with photoproduction amplitudes constructed from tree-level graphs are very flat. The peak structure appears only when the MB rescattering is taken into account in the final state, as the dashed red (for only WT graph) and continuous blue lines (for all graphs) show. In general, the inclusion of the Born terms moves the peak

structure to lower energies. We have also checked that the contribution of the anomalous graphs is relatively small. For this reason, we do not show their impact on the spectra separately to avoid overcrowding the figures with too many lines. We also conclude that at least at the c.m. energy $W = 2.0$ GeV the description of the $\pi^0\Sigma^0$ and $\pi^+\Sigma^-$ cross sections is quite reasonable. Although we cannot say the same about the $\pi^-\Sigma^+$ mass spectrum, one should bear in mind that our theoretical predictions are provided without any adjustment of the MB rescattering amplitudes that have a major impact on the calculated spectra but are generated by a model fitted to a completely different sector of experimental data and for much higher energies from the $\bar{K}N$ threshold up.

It is also well known that the chirally motivated $\bar{K}N$ models provide very different predictions for the energies

below the $\bar{K}N$ threshold as well as in the isovector sector [23]. Thus, we felt it necessary to check the sensitivity of the calculated $\pi\Sigma$ mass spectra to variations of the MB rescattering amplitudes. In Fig. 4 we show our results obtained at two sample energies, $W = 2.0$ (left figures) and 2.4 GeV (right figures), employing four different $\bar{K}N$ models that provide the final-state rescattering amplitudes f_{0+} required in Eq. (2.10). Besides the already mentioned Prague amplitudes [28], used to calculate the spectra shown in Fig. 3 and tagged as P model here, we also show results obtained with three versions of the Bonn model amplitudes: B2, B4 [26], and BW [60]. For $W = 2.0$ GeV, the continuous blue lines generated by the P model are exactly the same as those shown in Fig. 3.

The first impression one gets from Fig. 4 is that, taking aside the $\pi^0\Sigma^0$ and $\pi^+\Sigma^-$ results at $W = 2.0$ GeV, the

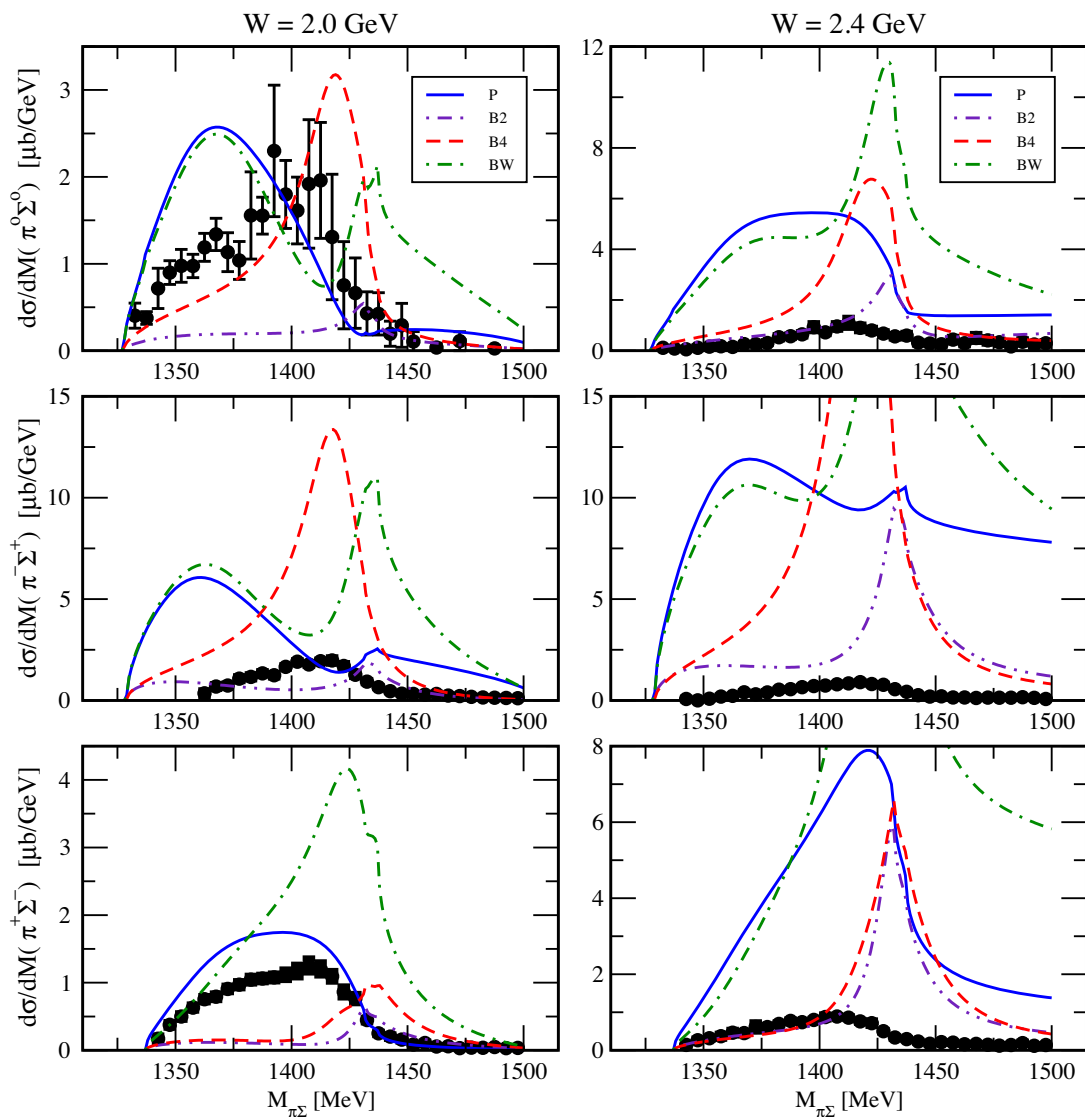


FIG. 4. Comparison of $\pi\Sigma$ mass distributions calculated at two c.m. energies, $W = 2.0$ and 2.4 GeV, while employing MB amplitudes generated by four different coupled-channel models tagged as P [28], B2, B4 [26], and BW [60]. The experimental data are taken from [30].

theoretical predictions provide much higher cross sections than those observed experimentally. We remark that similarly large cross sections of $d\sigma/dM_{\pi\Sigma} \approx 5\text{--}10 \mu\text{b}/\text{GeV}$ at the peak mass were predicted in the early Refs. [58,59] as well. As we will illustrate below, however, there is a hope that the magnitude of the $\pi\Sigma$ mass spectra can be reduced by tuning the rescattering contribution to the photoproduction amplitude. We also note that our formalism is based on LO ChPT which is expected to work much better at low energies. Specifically, a kaon momentum of $|\vec{q}_K|(W = 2 \text{ GeV}, M_{\pi\Sigma} = 1.35 \text{ GeV}) \approx 350 \text{ MeV}$ is still reasonable for three-flavor ChPT. However, at $W = 2.4 \text{ GeV}$ the kaon momentum is much larger, $|\vec{q}_K| \approx 717 \text{ MeV}$, probably too large for the LO ChPT photokernel. Therefore, the worse description of the observed mass distributions at $W = 2.4 \text{ GeV}$ can be anticipated.

It is interesting to note the close proximity of the theoretical predictions made with the P and BW model amplitudes. Despite the fact that the Prague and Bonn approaches to $\pi\Sigma - \bar{K}N$ coupled-channel interactions do differ significantly in several aspects, including the sets of experimental data their model parameters were fitted to, the P and BW models generate quite similar $\pi\Sigma$ photoproduction mass spectra up to about 1400 MeV. This can be understood by comparing the respective rescattering amplitudes which we demonstrate in Fig. 5. There, one can see that both models generate very similar MB amplitudes for energies up to the $\bar{K}N$ threshold.

The other two Bonn models, B2 and B4, were in fact used in fits that included the $\pi\Sigma$ photoproduction data from the CLAS experiment [26]. However, in those fits a simplified phenomenological approach was adopted to

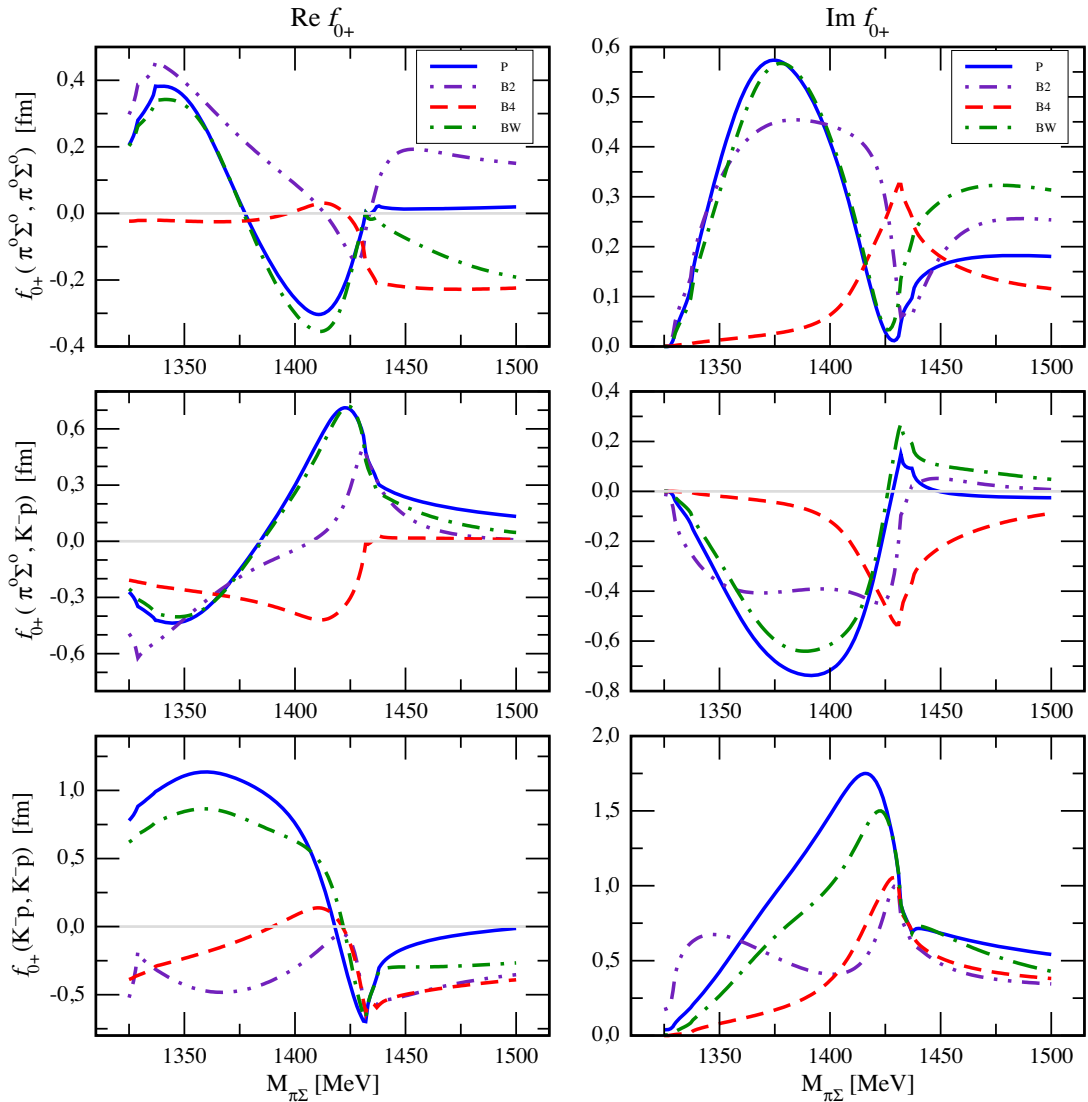


FIG. 5. The real (left) and imaginary (right) parts of s -wave scattering amplitudes for reactions $\pi^0\Sigma^0 \rightarrow \pi^0\Sigma^0$, $K^-p \rightarrow \pi^0\Sigma^0$, and $K^-p \rightarrow K^-p$. The amplitudes were generated by four different $\bar{K}N$ coupled-channel models specified in the text. The P model amplitude of the inelastic $K^-p \rightarrow \pi^0\Sigma^0$ process is shown with an opposite sign for an easier comparison with the other models.

model the photoproduction part (see also Ref. [34]) of the process in terms of makeshift energy-dependent constants used to multiply the amplitudes responsible for the MB rescattering in the final state. When compared with our present formulation of the photoproduction amplitude given in Eq. (2.10) the B2 and B4 models correspond to setting the tree graphs in the first term on the rhs to zero and (at the same time) replacing them by energy-dependent constants in the second term. It is obvious that such an *ad-hoc* treatment cannot reflect fully the complexity of the photoproduction process and the resulting MB amplitudes may not be quite reliable. However, the B2 and B4 amplitudes still describe the data well for K^-p reactions and represent a good option to test the model dependence of our theoretical predictions. Looking at Fig. 4 it seems that the available $\bar{K}N$ models are flexible enough to generate a peak in the $\pi\Sigma$ mass spectra at varied energies, and at least in the $\pi^-\Sigma^+$ channel provide even two peaks in case the data would support such option. The BW model predicts two peaks also in the $\pi^0\Sigma^0$ mass spectra, the one at higher mass quite close to the $\bar{K}N$ threshold where the chirally motivated approaches predict a resonance interpreted as a K^-p molecular state.

Coming back to the $\pi\Sigma$ mass spectra, we recall that generating the peak structures is only possible by including the MB rescattering in the final state as shown in Fig. 3. Algebraically, this is represented by the second term in Eq. (2.10) and one may consider modifications of either the rescattering amplitude or of the loop function that connects it to the tree-level photoproduction graphs. The first option would require a completely new fit to the experimental data including both the K^-p reactions data (at threshold and higher energies) as well as the $\pi\Sigma$ mass spectra discussed here. The complexity of such fits goes well beyond the scope of our current work, but we wish to illustrate how the magnitude of the photoproduction cross sections can be tuned by modifying the loop function $G(M_{\pi\Sigma})$ that enters Eq. (2.10). This is demonstrated in Fig. 6 where we present the results obtained with different choices of the regularization scales—the inverse range α for the P model and the mass scale μ in the case of the BW model. For simplicity, the same scale α or μ is used for all ten MB channels. The original mass spectra generated by the P and BW models (employing different regularization scales in different channels, matching those used to generate the rescattering amplitudes) are presented in the figure for comparison as well.

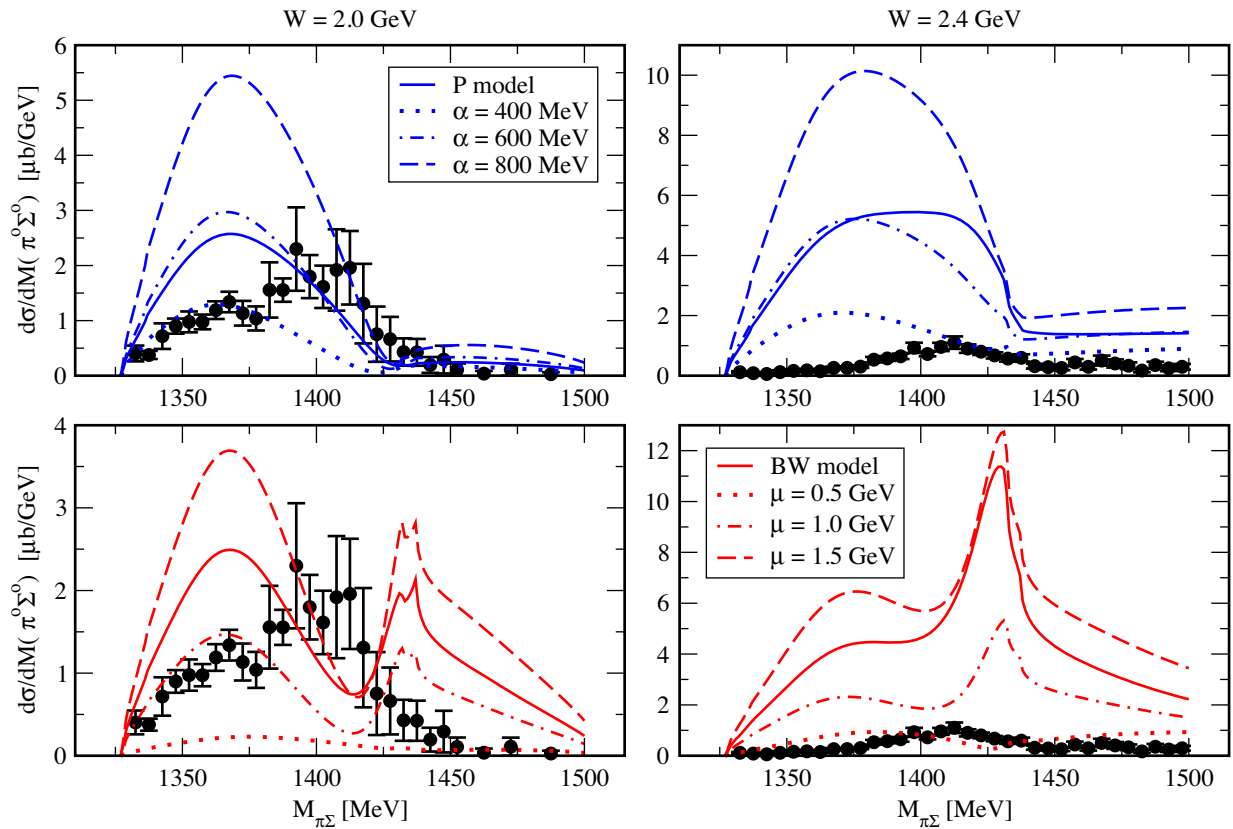


FIG. 6. A demonstration of the impact caused by modifying the regularization scales adopted in the loop functions connecting the tree-level photoproduction graphs with the meson-baryon rescattering amplitudes. The top (bottom) figures present the $\pi^0\Sigma^0$ mass spectra generated with the modified P model (BW model); the results obtained with the unmodified loop functions are shown for comparison as well.

The calculated spectra shown in Fig. 6 illustrate that lower values of the regularization scales α or μ lead to smaller cross sections. It seems that for $\alpha \approx 400$ MeV or for $\mu \approx 1.0$ GeV the magnitude of the generated $\pi\Sigma$ distributions is comparable to the one found in the CLAS experiment. Of course, the peak position and structure of the generated mass spectra require additional modifications that are driven by the energy dependence of the adopted f_{0+} amplitudes. As already stated, there is a room for such an adjustment since different MB coupled-channel models provide varied energy dependence of the amplitudes in between the $\pi\Sigma$ and $\bar{K}N$ thresholds.

At this point, one could consider the possibility of altering only the first MB loop function that appears in Eq. (2.10) while keeping unchanged the rescattering amplitudes and the loop functions used in coupled-channel approaches that generate them. Since the vertices connecting the photoproduction tree graphs with the MB rescattering part have a different structure than the $MB \rightarrow M'B'$ vertices, one can consider altering the first, e.g., by imposing additional form factors on them, while keeping the latter intact. Thus, the adopted modifications of the first loop functions that we used to tune the magnitude of the $\pi\Sigma$ cross sections can effectively relate to modifications of the \mathcal{M} vertex in Fig. 2. We note that a good reproduction of the CLAS data presented in Ref. [68] required a combined impact of modifications of the first MB loop functions, the addition of phenomenological contact terms contributing to the \mathcal{M} vertex as well as the addition of form factors applied to it.

Finally, we find it necessary to mention that the discussed CLAS data manifest variations between the mass distributions observed for the different $\pi\Sigma$ charge states. As it was already noted in [32] this indicates the existence of a substantial isovector strength in the $J^P = 1/2^-$ sector at energies overlapping with the $\Lambda(1405)$ resonance. In principle, such $I = 1$ contributions to the $\pi\Sigma$ mass spectra can be related to dynamically generated Σ^* resonances reported in some $\pi\Sigma - \bar{K}N$ coupled-channel models; see, e.g., [20,23,69]. Quite recently, it was also shown that the CLAS data can be reproduced with a model that includes baryon interactions with vector mesons in the final state and advocates the existence of a not yet established $\Sigma(1400)$ resonance [70]. Unfortunately, the isovector part of the MB interaction is not well determined in the current models, so its impact on the photoproduction mass spectra should be considered carefully and in context of a particular photoproduction model. At any case, the $d\sigma/M_{\pi\Sigma}$ data provide additional constraints on the MB coupled-channel approaches and this applies to their $I = 1$ sector too.

IV. SUMMARY AND CONCLUSION

In this article, we have outlined a methodology to incorporate the meson-baryon final-state interaction into the two-meson photoproduction amplitude through partial-wave amplitudes $f_{\ell\pm}$ constructed within the framework of

unitarized ChPT. This formalism can be used to implement coupled-channel unitarity, low-energy theorems from ChPT and gauge invariance in the description of the photoproduction process. Our results obtained with two versions of modern $\bar{K}N$ models, adopted to generate the MB amplitudes, demonstrate the crucial role played by the final-state interaction in the $\pi\Sigma$ photoproduction process. When the MB rescattering is omitted, only the considered tree graphs contribute to the photoproduction amplitude, and the generated cross sections are rather small and flat. The peak structure observed in the mass spectra reported by the CLAS Collaboration and related to a formation of the $\Lambda(1405)$ resonance appears only when the MB rescattering in the final state is accounted for in our formalism.

Our results show that the formalism is capable of reproducing the experimental data at c.m. energies $W \approx 2.0$ GeV where the pertinent kaon momenta are relatively small, complying with the limitations of three-flavor ChPT. The situation is worse at higher energies where our predictions provide too large cross sections when compared with the CLAS data. However, we would like to emphasize once again that these predictions are made without introducing any adjustment to the $\pi\Sigma - \bar{K}N$ coupled-channel models that were fitted to describe the data on K^-p reactions, at a completely different sector of kinematics and energies. We have also refrained from introducing any additional mechanisms in the tree-level photoproduction graphs that would go beyond the standard ChPT approach, nor applied any *ad-hoc* energy-dependent factors to moderate the generated mass spectra. In this sense our current predictions are completely parameter free. A much better agreement with the experimental data can be achieved by a combination of including the $\pi\Sigma$ photoproduction data in the fits of the $\bar{K}N$ models and maybe by applying an additional form factor to the \mathcal{M} vertex depicted in Fig. 2. Moreover, we have shown that adopting different $\bar{K}N$ models for the f_{0+} amplitudes leads to a varied structure of the computed $\pi\Sigma$ mass distributions that can accommodate spectra with either one or two peaks. As the line shapes of the charged $\pi\Sigma$ final states reflect an interference of the isoscalar and isovector contributions, including the $d\sigma/M_{\pi\Sigma}$ data in fits of the $\bar{K}N$ coupled-channel models should also help to determine the not-so-well established $I = 1$ part of the MB interaction. At the same time the magnitude of the calculated cross sections can be tuned by modifying the first MB loop function or the \mathcal{M} vertex.

Of course, it is also natural to ask about a role played by other kinds of final-state interaction inherent in the process, as, e.g., the pion-kaon interaction, irreducible three-body interactions, or even triangle-graph mechanisms as studied in Ref. [36]. In this respect we note that effects due to an enhanced final-state interaction in the other channels have already been subtracted in the CLAS data with which we compare our predictions [30]. There, it

was also reported that these effects have only a moderate impact on the $\pi\Sigma$ invariant mass spectra. Thus, it seems that a direct application of the approach proposed here is a reasonable strategy. In the future, one should also make efforts for a more complete description of the photoproduction process, along the lines explained so far. This would enable us to compare our predictions with a more complete subset of the provided data, as, e.g., the kaon angular distributions, which are presumably sensitive to final-state interaction in sectors not considered in this work.

ACKNOWLEDGMENTS

The work of P. C. B. and A. C. was supported by the Grant Agency of the Czech Republic under Grant No. 19-19640S. M. M. acknowledges support by the Deutsche Forschungsgemeinschaft (DFG, German Research Foundation) and the NSFC through the funds provided to the Sino-German Collaborative Research Center CRC 110 ‘‘Symmetries and the Emergence of Structure in QCD’’ (DFG Project-ID 196253076—TRR 110, NSFC Grant No. 12070131001).

APPENDIX: PROJECTION ON $\pi\Sigma$ PARTIAL WAVES

Here we provide explicit expressions for the s -wave projections of the photoproduction amplitude for $MB = \pi\Sigma$, but it is obvious that analogous expressions for the other meson-baryon channels can be found by simple replacements of the appropriate masses. As a first step, we define the combinations

$$\mathcal{C}_{0+}^1 = \mathcal{M}'_1 + (\sqrt{s} + m_N)\mathcal{M}'_5 + (\sqrt{s} - M_{\pi\Sigma})(\mathcal{M}'_9 + (\sqrt{s} + m_N)\mathcal{M}'_{13}), \quad (\text{A1})$$

$$\mathcal{C}_{0+}^2 = \mathcal{M}'_1 - (\sqrt{s} - m_N)\mathcal{M}'_5 - (\sqrt{s} + M_{\pi\Sigma})(\mathcal{M}'_9 - (\sqrt{s} - m_N)\mathcal{M}'_{13}), \quad (\text{A2})$$

$$\mathcal{C}_{0+}^3 = \mathcal{M}'_1 + (\sqrt{s} - M_{\pi\Sigma})\mathcal{M}'_9 + \frac{1}{2}(\sqrt{s} + m_N)(\mathcal{M}'_2 + (\sqrt{s} - m_N)\mathcal{M}'_6 + (\sqrt{s} - M_{\pi\Sigma})(\mathcal{M}'_{10} + (\sqrt{s} - m_N)\mathcal{M}'_{14})), \quad (\text{A3})$$

$$\mathcal{C}_{0+}^4 = \mathcal{M}'_1 - (\sqrt{s} + M_{\pi\Sigma})\mathcal{M}'_9 - \frac{1}{2}(\sqrt{s} - m_N)(\mathcal{M}'_2 - (\sqrt{s} + m_N)\mathcal{M}'_6 - (\sqrt{s} + M_{\pi\Sigma})(\mathcal{M}'_{10} - (\sqrt{s} + m_N)\mathcal{M}'_{14})), \quad (\text{A4})$$

employing the following abbreviations:

$$\mathcal{M}'_1 := \bar{\mathcal{M}}_1 - \frac{1}{3}(E_\Sigma^* - m_\Sigma)\bar{\mathcal{M}}_3, \quad \mathcal{M}'_5 := \bar{\mathcal{M}}_5 + \frac{1}{3}(E_\Sigma^* - m_\Sigma)\bar{\mathcal{M}}_7, \quad (\text{A5})$$

$$\mathcal{M}'_9 := \bar{\mathcal{M}}_9 + \frac{1}{3}(E_\Sigma^* - m_\Sigma)\bar{\mathcal{M}}_{11}, \quad \mathcal{M}'_{13} := \bar{\mathcal{M}}_{13} - \frac{1}{3}(E_\Sigma^* - m_\Sigma)\bar{\mathcal{M}}_{15}, \quad (\text{A6})$$

$$\mathcal{M}'_2 := \bar{\mathcal{M}}_2 + \frac{1}{3M_{\pi\Sigma}}(4E_\Sigma^* - m_\Sigma)\bar{\mathcal{M}}_3, \quad \mathcal{M}'_6 := \bar{\mathcal{M}}_6 + \frac{1}{3M_{\pi\Sigma}}(4E_\Sigma^* - m_\Sigma)\bar{\mathcal{M}}_7, \quad (\text{A7})$$

$$\mathcal{M}'_{10} := \bar{\mathcal{M}}_{10} + \frac{1}{3M_{\pi\Sigma}}(4E_\Sigma^* - m_\Sigma)\bar{\mathcal{M}}_{11}, \quad \mathcal{M}'_{14} := \bar{\mathcal{M}}_{14} + \frac{1}{3M_{\pi\Sigma}}(4E_\Sigma^* - m_\Sigma)\bar{\mathcal{M}}_{15}. \quad (\text{A8})$$

See Eq. (2.2) for the definition of the \mathcal{M}_i , and Eq. (2.8) for the definition of the $\bar{\mathcal{M}}_i$. We point out that the structure functions $\mathcal{M}_{4,8,12,16}$ are always eliminated via the gauge-invariance constraints

$$\begin{aligned} (s - m_N^2)\mathcal{M}_2 &\stackrel{!}{=} (u_\Sigma - m_\Sigma^2)\mathcal{M}_3 + (t_K - M_K^2)\mathcal{M}_4, \\ 2\mathcal{M}_1 + (s - m_N^2)\mathcal{M}_6 &\stackrel{!}{=} (u_\Sigma - m_\Sigma^2)\mathcal{M}_7 + (t_K - M_K^2)\mathcal{M}_8, \\ (s - m_N^2)\mathcal{M}_{10} &\stackrel{!}{=} (u_\Sigma - m_\Sigma^2)\mathcal{M}_{11} + (t_K - M_K^2)\mathcal{M}_{12}, \\ 2\mathcal{M}_9 + (s - m_N^2)\mathcal{M}_{14} &\stackrel{!}{=} (u_\Sigma - m_\Sigma^2)\mathcal{M}_{15} + (t_K - M_K^2)\mathcal{M}_{16}. \end{aligned} \quad (\text{A9})$$

In the simple case of structure functions \mathcal{M}_i independent of t_Σ , u_Σ , vanishing for $i = 3, 7, 11, 15$, we have $\mathcal{M}'_i = \mathcal{M}_i$. In fact, we can easily construct a gauge-invariant amplitude \mathcal{M}^μ of such a simplified form, which yields a set of prescribed $\mathcal{C}_{0+}^i(s, M_{\pi\Sigma}^2, t_K)$,

$$\mathcal{M}_1^c = \frac{1}{4\sqrt{s}M_{\pi\Sigma}} ((\sqrt{s} + M_{\pi\Sigma})(\sqrt{s} - m_N)\mathcal{C}_{0+}^1 - (\sqrt{s} - M_{\pi\Sigma})(\sqrt{s} + m_N)\mathcal{C}_{0+}^2), \quad (\text{A10})$$

$$\mathcal{M}_2^c = \frac{1}{2\sqrt{s}M_{\pi\Sigma}} ((\sqrt{s} + M_{\pi\Sigma})\mathcal{C}_{0+}^3 + (\sqrt{s} - M_{\pi\Sigma})\mathcal{C}_{0+}^4), \quad (\text{A11})$$

$$\mathcal{M}_3^c = 0, \quad (\text{A12})$$

$$\mathcal{M}_5^c = \frac{1}{4\sqrt{s}M_{\pi\Sigma}} ((\sqrt{s} + M_{\pi\Sigma})\mathcal{C}_{0+}^1 + (\sqrt{s} - M_{\pi\Sigma})\mathcal{C}_{0+}^2), \quad (\text{A13})$$

$$\mathcal{M}_6^c = \frac{1}{2\sqrt{s}M_{\pi\Sigma}} \left(\frac{\sqrt{s} + M_{\pi\Sigma}}{\sqrt{s} + m_N} (\mathcal{C}_{0+}^3 - \mathcal{C}_{0+}^1) + \frac{\sqrt{s} - M_{\pi\Sigma}}{\sqrt{s} - m_N} (\mathcal{C}_{0+}^2 - \mathcal{C}_{0+}^4) \right), \quad (\text{A14})$$

$$\mathcal{M}_7^c = 0, \quad (\text{A15})$$

$$\mathcal{M}_9^c = -\frac{1}{4\sqrt{s}M_{\pi\Sigma}} ((\sqrt{s} - m_N)\mathcal{C}_{0+}^1 + (\sqrt{s} + m_N)\mathcal{C}_{0+}^2), \quad (\text{A16})$$

$$\mathcal{M}_{10}^c = \frac{1}{2\sqrt{s}M_{\pi\Sigma}} (\mathcal{C}_{0+}^4 - \mathcal{C}_{0+}^3), \quad (\text{A17})$$

$$\mathcal{M}_{11}^c = 0, \quad (\text{A18})$$

$$\mathcal{M}_{13}^c = \frac{1}{4\sqrt{s}M_{\pi\Sigma}} (\mathcal{C}_{0+}^2 - \mathcal{C}_{0+}^1), \quad (\text{A19})$$

$$\mathcal{M}_{14}^c = \frac{1}{2\sqrt{s}M_{\pi\Sigma}} \left(\frac{\mathcal{C}_{0+}^1 - \mathcal{C}_{0+}^3}{\sqrt{s} + m_N} + \frac{\mathcal{C}_{0+}^2 - \mathcal{C}_{0+}^4}{\sqrt{s} - m_N} \right), \quad (\text{A20})$$

$$\mathcal{M}_{15}^c = 0, \quad (\text{A21})$$

with $\mathcal{M}_{4,8,12,16}^c$ accordingly fixed from the gauge-invariance constraints. Finally, we define

$$\begin{aligned} \mathcal{A}_{0+}^1 &:= \sqrt{E_{\Sigma}^* + m_{\Sigma}} \sqrt{E_{\pi\Sigma} + M_{\pi\Sigma}} (\mathcal{C}_{0+}^1) \sqrt{E_N - m_N} / \sqrt{2M_{\pi\Sigma}}, \\ \mathcal{A}_{0+}^2 &:= \sqrt{E_{\Sigma}^* + m_{\Sigma}} \sqrt{E_{\pi\Sigma} - M_{\pi\Sigma}} (\mathcal{C}_{0+}^2) \sqrt{E_N + m_N} / \sqrt{2M_{\pi\Sigma}}, \\ \mathcal{A}_{0+}^3 &:= \sqrt{E_{\Sigma}^* + m_{\Sigma}} \sqrt{E_{\pi\Sigma} + M_{\pi\Sigma}} (\mathcal{C}_{0+}^3) \sqrt{E_N - m_N} / \sqrt{2M_{\pi\Sigma}}, \\ \mathcal{A}_{0+}^4 &:= \sqrt{E_{\Sigma}^* + m_{\Sigma}} \sqrt{E_{\pi\Sigma} - M_{\pi\Sigma}} (\mathcal{C}_{0+}^4) \sqrt{E_N + m_N} / \sqrt{2M_{\pi\Sigma}}, \end{aligned}$$

where $E_{\pi\Sigma}$ is the c.m. energy of the $\pi\Sigma$ pair, $E_{\pi\Sigma} = \sqrt{s} - E_K = (s + M_{\pi\Sigma}^2 - M_K^2)/(2\sqrt{s})$. We also note that $|\vec{q}_K| = \sqrt{E_{\pi\Sigma}^2 - M_{\pi\Sigma}^2}$ and $E_N = (s + m_N^2)/(2\sqrt{s})$, $E_{\Sigma}^* = (M_{\pi\Sigma}^2 + m_{\Sigma}^2 - M_{\pi}^2)/(2M_{\pi\Sigma})$.

- [1] R. H. Dalitz and S. F. Tuan, A Possible Resonant State in Pion-Hyperon Scattering, *Phys. Rev. Lett.* **2**, 425 (1959).
- [2] M. H. Alston, L. W. Alvarez, P. Eberhard, M. L. Good, W. Graziano, H. K. Ticho, and S. G. Wojcicki, Study of Resonances of the $\Sigma - \pi$ System, *Phys. Rev. Lett.* **6**, 698 (1961).
- [3] T. Hyodo and D. Jido, The nature of the $\Lambda(1405)$ resonance in chiral dynamics, *Prog. Part. Nucl. Phys.* **67**, 55 (2012).
- [4] M. Mai, Review of the $\Lambda(1405)$ A curious case of a strangeness resonance, *Eur. Phys. J. Special Topics* **230**, 1593 (2021).
- [5] T. Hyodo and M. Niiyama, QCD and the strange baryon spectrum, *Prog. Part. Nucl. Phys.* **120**, 103868 (2021).
- [6] M. Mai, U.-G. Meißner, and C. Urbach, Towards a theory of hadron resonances, [arXiv:2206.01477](https://arxiv.org/abs/2206.01477).
- [7] L. Roca, M. Mai, E. Oset, and U.-G. Meißner, Predictions for the $\Lambda_b \rightarrow J/\psi \Lambda(1405)$ decay, *Eur. Phys. J. C* **75**, 218 (2015).
- [8] E. Oset *et al.*, Weak decays of heavy hadrons into dynamically generated resonances, *Int. J. Mod. Phys. E* **25**, 1630001 (2016).
- [9] V. Filippini *et al.* (FINUDA Collaboration), FINUDA, the physics program, *Nucl. Phys.* **A639**, 537 (1998).
- [10] M. Agnello *et al.* (FINUDA Collaboration), Evidence for a Kaon-Bound State K^-pp Produced in K^- Absorption Reactions at Rest, *Phys. Rev. Lett.* **94**, 212303 (2005).
- [11] T. Yamazaki *et al.* (DISTO Collaboration), First exclusive measurements of the K^-pp state populated in the $pp \rightarrow K^+ \Lambda p$ reaction at 2.85-GeV, *Hyperfine Interact.* **193**, 181 (2009).
- [12] M. Maggiora *et al.* (DISTO Collaboration), DISTO data on K^-pp , *Nucl. Phys.* **A835**, 43 (2010).
- [13] T. Yamazaki *et al.*, Indication of a Deeply Bound Compact K^-pp State Formed in the $pp \rightarrow p \Lambda K^+$ Reaction at 2.85 GeV, *Phys. Rev. Lett.* **104**, 132502 (2010).
- [14] Y. Sada *et al.* (J-PARC E15 Collaboration), Structure near $K^- + p + p$ threshold in the in-flight ${}^3\text{He}(K^-, \Lambda p)n$ reaction, *Prog. Theor. Exp. Phys.* **2016**, 051D01 (2016).
- [15] T. Yamaga *et al.* (J-PARC E15 Collaboration), Observation of a $\bar{K}NN$ bound state in the ${}^3\text{He}(K^-, \Lambda p)n$ reaction, *Phys. Rev. C* **102**, 044002 (2020).
- [16] A. Cieplý, E. Friedman, A. Gal, D. Gazda, and J. Mareš, K^- nuclear potentials from in-medium chirally motivated models, *Phys. Rev. C* **84**, 045206 (2011).
- [17] A. Gal, E. Friedman, N. Barnea, A. Cieplý, J. Mareš, and D. Gazda, In-medium K^- interactions and bound states, *EPJ Web Conf.* **81**, 01018 (2014).
- [18] J. Hrtánková, N. Barnea, E. Friedman, A. Gal, J. Mareš, and M. Schäfer, $\Lambda^*(1405)$ -matter: Stable or unstable?, *Phys. Lett. B* **785**, 90 (2018).
- [19] A. Gal, E. V. Hungerford, and D. J. Millener, Strangeness in nuclear physics, *Rev. Mod. Phys.* **88**, 035004 (2016).
- [20] J. A. Oller and U.-G. Meißner, Chiral dynamics in the presence of bound states: Kaon nucleon interactions revisited, *Phys. Lett. B* **500**, 263 (2001).
- [21] D. Jido, J. A. Oller, E. Oset, A. Ramos, and U.-G. Meißner, Chiral dynamics of the two $\Lambda(1405)$ states, *Nucl. Phys.* **A725**, 181 (2003).
- [22] M. Mai and U.-G. Meißner, New insights into antikaon-nucleon scattering and the structure of the $\Lambda(1405)$, *Nucl. Phys.* **A900**, 51 (2013).
- [23] A. Cieplý, M. Mai, U.-G. Meißner, and J. Smejkal, On the pole content of coupled channels chiral approaches used for the $\bar{K}N$ system, *Nucl. Phys.* **A954**, 17 (2016).
- [24] Y. Ikeda, T. Hyodo, and W. Weise, Chiral SU(3) theory of antikaon-nucleon interactions with improved threshold constraints, *Nucl. Phys.* **A881**, 98 (2012).
- [25] Z.-H. Guo and J. A. Oller, Meson-baryon reactions with strangeness -1 within a chiral framework, *Phys. Rev. C* **87**, 035202 (2013).
- [26] M. Mai and U.-G. Meißner, Constraints on the chiral unitary $\bar{K}N$ amplitude from $\pi \Sigma K^+$ photoproduction data, *Eur. Phys. J. A* **51**, 30 (2015).
- [27] A. Feijoo, V. Magas, and A. Ramos, $S = -1$ meson-baryon interaction and the role of isospin filtering processes, *Phys. Rev. C* **99**, 035211 (2019).
- [28] P. C. Bruns and A. Cieplý, SU(3) flavor symmetry considerations for the K^-N coupled channels system, *Nucl. Phys.* **A1019**, 122378 (2022).
- [29] U.-G. Meißner, Two-pole structures in QCD: Facts, not fantasy!, *Symmetry* **12**, 981 (2020).
- [30] K. Moriya *et al.* (CLAS Collaboration), Measurement of the $\Sigma\pi$ photoproduction line shapes near the $\Lambda(1405)$, *Phys. Rev. C* **87**, 035206 (2013).
- [31] R. A. Schumacher and K. Moriya, Isospin decomposition of the photoproduced $\Sigma\pi$ system near the $\Lambda(1405)$, *Nucl. Phys.* **A914**, 51 (2013).
- [32] K. Moriya *et al.* (CLAS Collaboration), Differential photoproduction cross sections of the $\Sigma^0(1385)$, $\Lambda(1405)$, and $\Lambda(1520)$, *Phys. Rev. C* **88**, 045201 (2013); **88**, 049902(A) (2013).
- [33] L. Roca and E. Oset, Isospin 0 and 1 resonances from $\pi\Sigma$ photoproduction data, *Phys. Rev. C* **88**, 055206 (2013).
- [34] L. Roca and E. Oset, $\Lambda(1405)$ poles obtained from $\pi^0\Sigma^0$ photoproduction data, *Phys. Rev. C* **87**, 055201 (2013).
- [35] S. X. Nakamura and D. Jido, $\Lambda(1405)$ photoproduction based on chiral unitary model, *Prog. Theor. Exp. Phys.* **2014**, 023D01 (2014).
- [36] E. Wang, J.-J. Xie, W.-H. Liang, F.-K. Guo, and E. Oset, Role of a triangle singularity in the $\gamma p \rightarrow K^+ \Lambda(1405)$ reaction, *Phys. Rev. C* **95**, 015205 (2017).
- [37] S. Nam, Photo- and electroproduction of $\Lambda(1405)$ via $\gamma^{(*)} p \rightarrow K^+ \pi^+ \Sigma^-$, *Phys. Rev. D* **96**, 076021 (2017).
- [38] A. V. Anisovich, A. V. Sarantsev, V. A. Nikonov, V. Burkert, R. A. Schumacher, U. Thoma, and E. Klempt, Hyperon III: $K^-p - \pi\Sigma$ coupled-channel dynamics in the $\Lambda(1405)$ mass region, *Eur. Phys. J. A* **56**, 139 (2020).
- [39] A. V. Anisovich, Excitation of hyperon resonances in photoproduction, *Eur. Phys. J. A* **57**, 236 (2021).
- [40] P. C. Bruns, A formalism for the study of $K^+ \pi\Sigma$ photoproduction in the $\Lambda^*(1405)$ region, [arXiv:2012.11298](https://arxiv.org/abs/2012.11298).
- [41] I. Zychor *et al.*, Shape of the $\Lambda(1405)$ hyperon measured through its $\Sigma^0 \pi^0$ Decay, *Phys. Lett. B* **660**, 167 (2008).
- [42] G. Scheluchin *et al.* (BGOOD Collaboration), Photoproduction of $K^+ \Lambda(1405) \rightarrow K^+ \pi^0 \Sigma^0$ extending to forward angles and low momentum transfer, *Phys. Lett. B* **833**, 137375 (2022).

- [43] G. Agakishiev *et al.* (HADES Collaboration), Baryonic resonances close to the $\bar{K}N$ threshold: The case of $\Lambda(1405)$ in pp collisions, *Phys. Rev. C* **87**, 025201 (2013).
- [44] N. Wickramaarachchi (GlueX Collaboration), Decay of the $\Lambda(1405)$ to $\Sigma^0\pi^0$ measured at GlueX, in *Proceedings of the HYP2022 Conference in Prague, Czechia, 2022* (2022) [arXiv:2209.06230].
- [45] M. Bazzi *et al.* (SIDDHARTA Collaboration), Preliminary study of kaonic deuterium X-rays by the SIDDHARTA experiment at DAΦNE, *Nucl. Phys.* **A907**, 69 (2013).
- [46] C. Curceanu *et al.*, Unlocking the secrets of the kaon-nucleon/nuclei interactions at low-energies: The SIDDHARTA(-2) and the AMADEUS experiments at the DAΦFNE collider, *Nucl. Phys.* **A914**, 251 (2013).
- [47] J. Marton *et al.*, Low-energy antikaon interaction with nuclei: The AMADEUS challenge, *J. Phys. Soc. Jpn. Conf. Proc.* **18**, 011034 (2017).
- [48] M. Amaryan *et al.* (KLF Collaboration), Strange hadron spectroscopy with secondary KL beam in Hall D, arXiv:2008.08215.
- [49] M. F. M. Lutz *et al.* (PANDA Collaboration), Physics performance report for PANDA: Strong interaction studies with antiprotons, arXiv:0903.3905.
- [50] G. Barucca *et al.* (PANDA Collaboration), PANDA phase one, *Eur. Phys. J. A* **57**, 184 (2021).
- [51] J. Wess and B. Zumino, Consequences of anomalous Ward identities, *Phys. Lett.* **37B**, 95 (1971).
- [52] E. Witten, Global aspects of current algebra, *Nucl. Phys.* **B223**, 422 (1983).
- [53] R. E. Cutkosky, Singularities and discontinuities of Feynman amplitudes, *J. Math. Phys. (N.Y.)* **1**, 429 (1960).
- [54] G. F. Chew, M. L. Goldberger, F. E. Low, and Y. Nambu, Application of dispersion relations to low-energy meson-nucleon scattering, *Phys. Rev.* **106**, 1337 (1957).
- [55] G. F. Chew, M. L. Goldberger, F. E. Low, and Y. Nambu, Relativistic dispersion relation approach to photomeson production, *Phys. Rev.* **106**, 1345 (1957).
- [56] L. D. Pearlstein and A. Klein, Transition amplitudes for photoproduction of mesons from nucleons and photodisintegration of the deuteron, *Phys. Rev.* **107**, 836 (1957).
- [57] F. A. Berends, A. Donnachie, and D. L. Weaver, Photoproduction and electroproduction of pions. 1. Dispersion relation theory, *Nucl. Phys.* **B4**, 1 (1967).
- [58] J. C. Nacher, E. Oset, H. Toki, and A. Ramos, Photoproduction of the $\Lambda(1405)$ on the proton and nuclei, *Phys. Lett. B* **455**, 55 (1999).
- [59] M. F. M. Lutz and M. Soyeur, The associated photoproduction of positive kaons and $\pi^0\Lambda$ or $\pi\Sigma$ pairs in the region of the $\Sigma(1385)$ and $\Lambda(1405)$ resonances, *Nucl. Phys.* **A748**, 499 (2005).
- [60] D. Sadasivan, M. Mai, and M. Döring, S- and p-wave structure of $S = -1$ meson-baryon scattering in the resonance region, *Phys. Lett. B* **789**, 329 (2019).
- [61] P. C. Bruns and A. Cieplý, Coupled channels approach to ηN and $\eta' N$ interactions, *Nucl. Phys.* **A992**, 121630 (2019).
- [62] C. H. M. van Antwerpen and I. R. Afnan, A gauge invariant unitary theory for pion photoproduction, *Phys. Rev. C* **52**, 554 (1995).
- [63] B. Borasoy, P. C. Bruns, U.-G. Meißner, and R. Nißler, Gauge invariance in two-particle scattering, *Phys. Rev. C* **72**, 065201 (2005).
- [64] B. Borasoy, P. C. Bruns, U.-G. Meißner, and R. Nißler, A gauge invariant chiral unitary framework for kaon photo- and electroproduction on the proton, *Eur. Phys. J. A* **34**, 161 (2007).
- [65] M. Mai, P. C. Bruns, and U.-G. Meißner, Pion photoproduction off the proton in a gauge-invariant chiral unitary framework, *Phys. Rev. D* **86**, 094033 (2012).
- [66] H. Haberzettl, K. Nakayama, and Y.-S. Oh, Theory of two-meson photo- and electroproduction off the nucleon, *Phys. Rev. D* **99**, 053001 (2019).
- [67] H. Haberzettl, Gauge invariance of meson photo- and electroproduction currents revisited, *Phys. Rev. D* **104**, 056001 (2021).
- [68] S. X. Nakamura, H. Kamano, and T. Sato, Dynamical coupled-channels model for neutrino-induced meson productions in resonance region, *Phys. Rev. D* **92**, 074024 (2015).
- [69] K. P. Khemchandani, A. Martínez Torres, and J. A. Oller, Hyperon resonances coupled to pseudoscalar- and vector-baryon channels, *Phys. Rev. C* **100**, 015208 (2019).
- [70] S.-H. Kim, K. P. Khemchandani, A. Martínez Torres, S.-i. Nam, and A. Hosaka, Photoproduction of Λ^* and Σ^* resonances with $J^P = 1/2^-$ off the proton, *Phys. Rev. D* **103**, 114017 (2021).